26

The Fluid Mechanics of Premelted Liquid Films

M. G. WORSTER AND J. S. WETTLAUFER

26.1. Introduction

It is a well-known fluid-mechanical phenomenon that a droplet of one fluid immersed in another migrates up an imposed temperature gradient (Levich, 1962). Such thermophoresis is effected by thermocapillarity – the surface tension between two fluids is a decreasing function of temperature, so thermal gradients give rise to tangential stresses at a fluid–fluid interface. Thermophoresis of solid particles immersed in a fluid can also occur, driven, for example, by gradients in the strength of a surrounding electrical double layer (Anderson, 1989). The converse, a fluid droplet migrating through a solid under the influence of an ambient temperature gradient, can occur by a process of melting and resolidification. Sometimes known as temperature gradient zone migration (TGZM), this was the subject of a talk by Yih at the GI Taylor Memorial Symposium in 1987 that one of us (MGW) was privileged to hear (Yih, 1986, 1987). This chapter describes the fundamental mechanisms underlying a related process, thermal regelation, by which a solid particle immersed in another solid can migrate up an imposed temperature gradient. Thermal regelation is similar to TGZM in that it involves melting and resolidification of the surrounding solid. However, whereas in TGZM the melting (really dissolution) is caused by solute gradients within the liquid inclusion, in thermal regelation the melting is caused by intermolecular forces (such as van der Waals forces) altering the equilibrium states of matter near interfaces. Specifically, although a material held in thermodynamic equilibrium below its bulk freezing temperature is solid in the main, it may nevertheless be liquid in a thin layer adjacent to its contact with a foreign substrate.

That such (premelted) liquid films might exist was suggested by Faraday (1860) and can be predicted from interfacial thermodynamics (e.g., Lipowsky, 1982; 1984). More recently, direct evidence of their existence has come from a number of different experiments (see Dash, et al., 1995, for a review). Such experiments reveal the breakdown of long-range periodic order at the surface of a crystalline solid, where it makes contact either with its own vapor or with a foreign substrate. That this disordered state, which has been variously referred to as quasi-liquid or as being liquidlike (e.g., Löwen et al., 1989), is fluid is implicit in any understanding of thermal regelation and other related phenomena. There is now, however, explicit experimental evidence that premelted liquid flows in response to an applied temperature gradient (Wilen and Dash, 1995). Further, fluid-mechanical calculations based on an assumption that the premelted liquid behaves as a Newtonian fluid with the same viscosity as the bulk molten material are adequate to predict the results of the experiments.

In this chapter we describe the thermodynamic arguments used to predict premelting and to calculate the relationship between pressure and temperature in premelted liquid films. We review some of the calculations made of flows involving premelted films, including thermal

regelation, and introduce a new model, based on these and additional premelting effects, of the growth of an ice lens in a water-saturated soil – a process fundamental to the phenomenon of frost heave.

Premelting can be induced by a variety of intermolecular forces. For uniformity of presentation we discuss only the case of van der Waals forces. The fluid-mechanical processes we describe and the associated free-boundary problems are similar in the other cases.

26.2. Premelting due to van der Waals Forces

We present here an outline of the physical principles underlying the phenomenon of premelting sufficient to determine the fluid pressure driving the flows examined in the remainder of the chapter. For a more precise and detailed treatment, see Wettlaufer and Worster (1995).

Consider a semi-infinite solid (s) separated by its own melt (m) from a semi-infinite substrate (w). The van der Waals forces between all the molecules in the three layers give rise to a force per unit area between the solid and the substrate (the thermomolecular pressure):

$$p_T = \frac{A}{6\pi d^3}, \tag{1}$$

where d is the thickness of the liquid film. The effective Hamaker constant A depends on the dielectric properties of all three materials in the layered system and can have either sign (Tabor, 1991). The pressure represented by Eq. (1) is familiar in the context of thin-film fluid mechanics and can, for example, lead to rupturing of a liquid film on a solid substrate when A is negative and the interfacial interaction is therefore attractive.

We are interested in cases in which A is positive so that there is a force of repulsion (disjoining pressure) between the media bounding the liquid film. The external pressure applied to the substrate p_w, equal to that applied to the solid p_s, balances the thermomolecular pressure p_T and the hydrodynamic pressure p_l. Thus

$$p_w = p_s = p_T + p_l. \tag{2}$$

Finally, the Gibbs–Duhem relationship can be applied on each side of a solid–melt interface to show in general that in equilibrium

$$p_s - p_l = \frac{\rho_s q (T_m - T)}{T_m}, \tag{3}$$

where ρ_s is the density of the solid, q is the latent heat of solidification per unit mass, T_m is the bulk melting temperature of the solid, and T is the temperature of the system.

Combining Eqs. (1)–(3) shows that the equilibrium thickness of the liquid film is

$$d = \lambda \left(\frac{T_m - T}{T_m} \right)^{-1/3}, \tag{4}$$

where $\lambda^3 = A/6\pi\rho_s q$. Equation (4), which shows that a premelted liquid film can exist (when $A > 0$) at temperatures below the bulk freezing point and gives the relationship between its thickness and the temperature, has received experimental confirmation for many different materials (Dash et al., 1995).

26.3. Flow of Premelted Liquid

Equation (4) shows that the thickness of a premelted liquid film decreases as the temperature decreases. Correspondingly, the thermomolecular pressure increases. Thus, if the external pressure is held constant, for example, then the pressure in the liquid decreases and there is a tendency for premelted liquid to flow from warmer to cooler regions.

An experiment to investigate premelting by measuring such a flow was designed by Wilen and Dash (1995). In it, water was sandwiched in a cylindrical layer between a lower glass slide and a flexible upper membrane, from the center to the outside of which was imposed a steady temperature gradient (Fig. 26.1). The axis of the cylindrical layer was held at a temperature below the bulk freezing temperature (0°C), causing a disk of ice to grow radially outward until its edge coincided with the 0°C isotherm. Without premelting, this would have been the ultimate steady configuration of the system. However, the thermomolecular pressure gradients in the premelted liquid film between the ice and the flexible membrane drew water radially inward, which resulted in the membrane being deflected laterally. In order to maintain the equilibrium thickness of the premelted film, the additional water froze onto the upper surface of the disk of ice.

This process can be modeled simply, with lubrication theory to analyze the flow in the premelted liquid film (Wettlaufer et al., 1996). The membrane is significantly displaced only

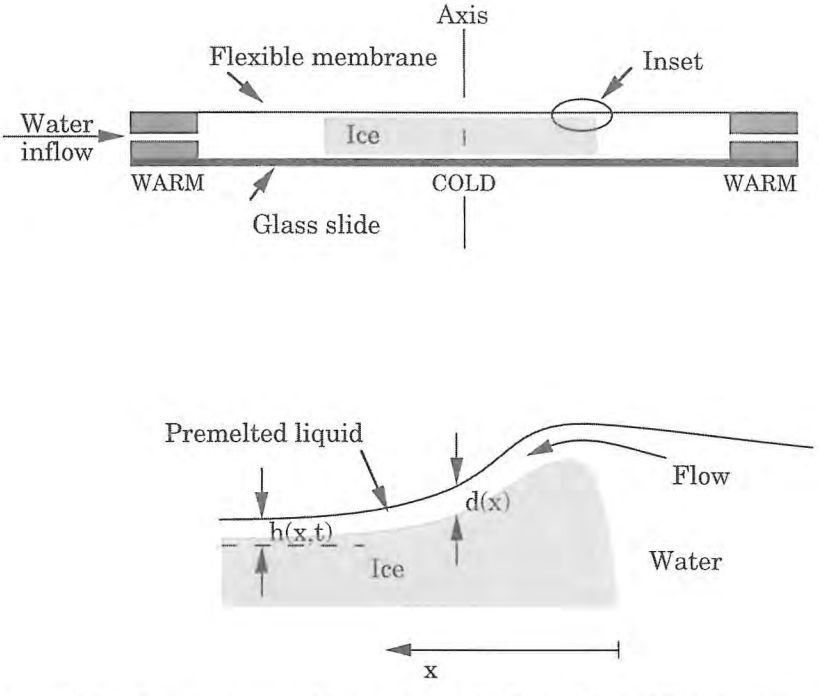

Figure 26.1. Schematic diagram of the experiment of Wilen and Dash (1995), showing an axial cross section through a cylindrical apparatus. A disk of ice grew radially outward between a lower glass slide and an upper flexible membrane until its outer edge coincided with the 0°C isotherm. The pressure gradient in the premelted liquid between the ice and the membrane drew water radially inward, as shown in the inset, which has a greatly exaggerated vertical scale.

near the rim of the disk of ice, so a two-dimensional analysis of a radial cross section is sufficient to model the experiments.

The temperature field is steady and given by

$$T = T_m - Gx,$$

where G is the constant imposed temperature gradient and x is distance from the leading edge of the ice toward the center of the disk. The volumetric flow rate q per unit length transverse to the flow in the premelted liquid film is given by lubrication theory to be

$$q = -\frac{d^3}{12\mu}\frac{\partial p_l}{\partial x} = -\frac{\lambda^3 T_m}{12\mu G x}\frac{\partial p_l}{\partial x}. \tag{5}$$

For small wall displacement $h(x, t)$, the pressure exerted by the elastic membrane is

$$p_w \approx -\gamma h_{xx}, \tag{6}$$

where γ is the tension in the membrane. So from Eqs. (2) and (3), the liquid pressure is

$$p_l = -\gamma h_{xx} - \frac{\rho_s q}{T_m} Gx. \tag{7}$$

Combining Eqs. (5) and (7) into the conservation equation

$$h_t + q_x = 0 \tag{8}$$

leads to the evolution equation for the wall displacement

$$h_t + D[x^{-1}(h_{xxx} + \beta)]_x = 0, \tag{9}$$

where

$$D = \frac{1}{12}\frac{\lambda^3 T_m}{G}\frac{\gamma}{\mu}, \qquad \beta = \frac{\rho_s q G}{\gamma T_m}.$$

Equation (9) admits a similarity solution,

$$h = \beta(Dt)^{3/5} f(\eta), \qquad \text{with} \quad \eta = \frac{x}{(Dt)^{1/5}},$$

where the dimensionless wall displacement satisfies

$$f'''' - \frac{f''' + 1}{\eta} - \frac{1}{5}\eta^2 f' + \frac{3}{5}\eta f = 0 \tag{10}$$

and boundary conditions

$$f' = f'' = 0 \quad (\eta = 0), \qquad f \to 0 \quad (\eta \to \infty). \tag{11}$$

The solution of this ordinary-differential system is displayed in Fig. 26.2.

All the physical parameters in this theory are known independently of the experiments of Wilen and Dash (1995), with the exception of λ. Additionally, it has often been speculated that, although premelted liquid behaves as a Newtonian fluid (Mantovani et al., 1980), its viscosity may be significantly different from that of bulk liquid. Since λ and μ appear only in ratio, in the parameter D, it is not possible to use these experiments to determine values for λ and

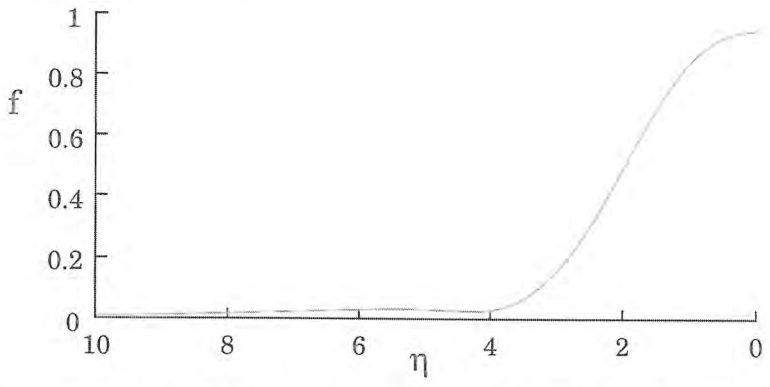

Figure 26.2. The similarity solution for the deflection f of the flexible membrane shown in Fig. 26.1, where η is a scaled x coordinate. The deformation is largest at high temperatures at which the gradient of volume flux is largest. Typical physical parameter values give a horizontal-to-vertical aspect ratio of a few hundred.

μ separately. Wettlaufer et al. (1996) presented a family of similarity solutions for different power-law interactions (including the case of van der Waals) and found good agreement with the experimental results when $p_T \propto d^{-2}$, corresponding to long-range electrostatic interactions. Assuming that the viscosity of the premelted liquid is the same as that of bulk liquid led them to a prediction for the multiplicative constant (the equivalent of λ) consistent with independent calculations (Wilen et al., 1995) suggesting that the bulk value of viscosity is appropriate. A similar conclusion was drawn by Gilpin (1980) from wire-regelation experiments, which are discussed in Section 26.4 below.

26.4. Thermal Regelation

A solid particle encased in ice, for example, migrates toward warmer regions of the ice. This phenomenon was analyzed by Gilpin (1979) alongside the closely related problem of pressure-induced regelation, whereby a weighted wire is pulled through a block of ice.* Although the latter can be effected by pressure melting (the decrease in bulk freezing temperature of ice under pressure), it was shown by Telford and Turner (1963) that regelation still occurs at temperatures and pressures too low for pressure melting to operate. Both pressure-induced regelation and thermal regelation can be explained in terms of premelting. The description given here follows closely that of Gilpin (1979), although expressed in terms of van der Waals interactions rather than a spatially varying chemical potential.

Consider a solid sphere of radius a surrounded by ice, as shown in Fig. 26.3. We assume that the thermal properties of the sphere, ice, and premelted water are identical and that the latent heat released and absorbed as the sphere migrates is negligible. The temperature is then given everywhere by

$$T = T_0 + Gx = T_0 - Ga\cos\theta, \tag{12}$$

where T_0 is the temperature at the center of the sphere, x is measured upward from the center

* The term regelation was used by Tyndall (1858) and Faraday (1860) to describe the sintering of ice crystals by the freezing of (premelted) liquid layers on their surfaces.

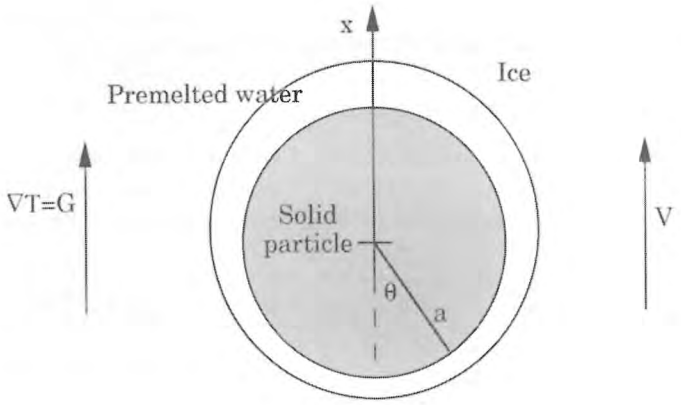

Figure 26.3. A definition sketch for the migration of a solid particle through a block of ice by the process of thermal regelation.

of the sphere, and θ is the polar angle measured from the downward vertical. Therefore, if the dominant intermolecular interactions are van der Waals, this temperature field gives rise to a premelted liquid film around the sphere of thickness:

$$d = \lambda T_m^{1/3}(T_m - T_0 + Ga\cos\theta)^{-1/3}. \tag{13}$$

The thermomolecular pressure within this film,

$$p_T = \frac{\rho_s q}{T_m}(T_m - T_0 + Ga\cos\theta),$$

provides a net upward force on the sphere:

$$F_T = \frac{4\pi a^3}{3}\frac{\rho_s q}{T_m}G. \tag{14}$$

Mass conservation during steady migration of the sphere at speed V gives the local volumetric flow rate per unit length transverse to the flow in the thin film to be

$$q = -\frac{1}{2}a\sin\theta V = -\frac{d^3}{12\mu}\frac{1}{a}\frac{\partial p_l}{\partial\theta}. \tag{15}$$

The latter equation, derived from lubrication theory, can be readily integrated to give

$$p_l = p_0 - \frac{6\mu a^2 V}{\lambda^3 T_m}\left(T_m - T_0 + \frac{1}{2}Ga\cos\theta\right)\cos\theta,$$

whence the net upward lubrication force on the sphere can be calculated to be

$$F_\mu = -\frac{4\pi a^3}{3}\frac{6\mu a V}{\lambda^3}\left(\frac{T_m - T_0}{T_m}\right). \tag{16}$$

If there is an external force on the particle, for example if the sphere is heavier than water, then there is an overburden force,

$$F_O = -\frac{4\pi a^3}{3}\Delta\rho g, \tag{17}$$

where $\Delta\rho$ is the density difference between particle and water and g is the acceleration due to gravity. The total force $F_T + F_\mu + F_O$ is zero, so the migration velocity can be determined to be

$$V = \frac{\lambda^3}{6\mu a}\frac{T_m}{T_m - T_0}\left[\frac{\rho_s q}{T_m}G - \Delta\rho g\right]. \tag{18}$$

This is perhaps the simplest expression embodying the processes of thermal regelation ($g = 0$) and pressure-induced regelation ($G = 0$) and shows the dominant physical parameters controlling these phenomena. In order to make quantitative comparisons with experiments, however, a more detailed analysis is required that accounts for the different thermal properties of the different phases, the release of latent heat, pressure melting, and the effects of any dissolved solutes (e.g., Nye, 1967).

26.5. Particle Rejection

A similar analysis to that presented above can be used to explain how solid particles can be pushed ahead of a solidification front. It is known from experiments that particles suspended in a melt are pushed ahead of the front if the solidification rate is sufficiently slow but become engulfed when the solidification rate exceeds a critical rate V_c (e.g., Azouni et al., 1990; Lipp et al., 1990; Lipp and Körber 1993).

In many analyses of this phenomenon it is assumed that the solidification front is planar. It is straightforward then to determine the van der Waals repulsion and to calculate the lubrication pressure from an analysis of the squeeze film between the ice and particle (assumed spherical). However, given this too-simple picture, it is not possible to determine the distance between the particle and the solidification front. Therefore the critical velocity V_c cannot be determined either, although one can place a rather extreme bound on it by taking the distance of separation to be equal to the molecular cutoff distance for the van der Waals force. As the particle nears the solidification front, however, interfacial premelting causes the front to become concave toward the liquid and thus to begin to conform to the particle (Fig. 26.4). The lubrication force then increases markedly to a point where it can no longer be balanced by the van der Waals repulsion and the particle becomes engulfed. This effect of a nonplanar interface is widely recognized and has been incorporated in many analyses, although often the deflection of the interface has been attributed to dissolved solutes or to the difference in the thermal conductivities of the particle and the ice. Note that the latter effect can cause the interface to deflect either way, depending on the relative conductivities, and it retards engulfment if the particle is less conductive than the ice (Chernov, et al., 1977). Recent experiments (Azouni et al., 1997) indicate that particle trapping depends dominantly on the nature of the surface of the particle, which suggests that bulk thermal and solutal effects are not the primary mechanism controlling engulfment.

An analysis of particle rejection based purely on the effects of premelting can be distilled from the work of Chernov et al. (1977). Equations (4) and (12) applied to the solidification front combine to yield

$$\frac{l^4}{d^3} = (a + d)\cos\theta - H, \tag{19}$$

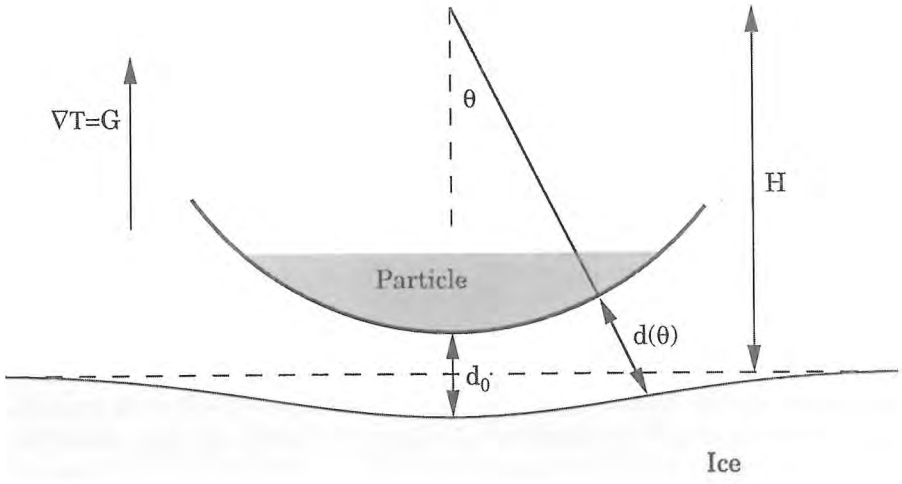

Figure 26.4. A definition sketch for the rejection of a solid particle from an advancing ice–water interface. Note that, in steady state, with the interface advancing at a fixed rate V, the particle rides higher than the undisturbed location of the interface. Premelting causes the interface to be deformed beneath the particle, which increases the lubrication pressure there and ultimately results in the particle being engulfed.

where $H = (T_0 - T_m)/G$ is the vertical distance between the center of the sphere and the undisturbed location of the solidification front (which is at the bulk melting isotherm), d is the radial distance between the particle and the solidification front, and l is a length scale given by

$$l^4 = \frac{\lambda^3 T_m}{G}. \tag{20}$$

The van der Waals force and the lubrication force are both locally dominated by the neiborhood of $\theta = 0$. Equation (19) can be differentiated twice to show that

$$d \approx d_0 + \frac{\frac{1}{2}a\theta^2}{1 + \frac{3l^4}{d_0^4}} \qquad \text{for} \quad \theta \ll 1, \tag{21}$$

where d_0 is the minimum thickness of the liquid film. With this approximate expression for d, the van der Waals and lubrication forces are readily calculated to be

$$F_T \approx \frac{Aa}{6d_0^2}\left(1 + \frac{3l^4}{d_0^4}\right), \tag{22}$$

$$F_\mu \approx -\frac{6\pi\mu a^2 V}{d_0}\left(1 + \frac{3l^4}{d_0^4}\right)^2. \tag{23}$$

The net force on the particle is zero, so approximations (22) and (23) show that

$$V = \frac{A}{36\pi\mu a}\frac{d_0^3}{d_0^4 + 3l^4}. \tag{24}$$

Given a solidification rate V, this equation can be used to determine the distance d_0 at which a steady equilibrium is achieved between the van der Waals and the hydrodynamic forces, which are augmented by the conformity of the phase boundary to the particle induced by premelting. If V is too large, Eq. (24) has no solution; no equilibrium is then possible and the particle is engulfed.

Maximizing V, as given by Eq. (24), with respect to d_0 gives the critical solidification rate:

$$V_c = \frac{\sqrt{3}}{144\pi}\frac{A}{\mu a l} = \frac{\sqrt{3}}{24}\frac{\rho_s q \lambda^{9/4}}{\mu T_m^{1/4}}\frac{G^{1/4}}{a}. \tag{25}$$

There is significant experimental support for the relationship $V_c \propto a^{-1}$ and some support for the relationship $V_c \propto G^{1/4}$, although there is also evidence in favor of other exponents in the latter expression (Pötschke and Rogge, 1989; Lipp and Körber, 1993). Note that, at the critical solidification rate, $d_0 = \sqrt{3}l$ whereas the deflection of the interface is only $l/3\sqrt{3}$, so the particle sits above the undisturbed position of the interface, as shown in Fig. 26.4.

Note that the critical solidification rate provides a different relationship between viscosity and the Hamaker constant, which, in principle, can be used in combination with the earlier result to determine values for these quantities separately.

26.6. Ice Lenses

The fundamental physical mechanisms discussed above underlie a unique environmental problem: frost heave. When a saturated soil is cooled below the freezing temperature of the interstitial water, it can undergo large-scale deformations. The total deformation of the partially frozen soil is accounted for by a sequence of ice lenses (layers of ice from which all the soil particles have been expelled) that form perpendicularly to the temperature gradient. Ice lenses typically form periodically in a frozen soil but it is possible, by cooling very slowly, to form a single, continuous ice lens, as illustrated in Fig. 26.5(a) (T. Ishizaki, private communication). This situation is similar to the particle rejection just discussed but differs in some important respects. Equation (19) is an approximate form of the more general interface condition

$$T_m - T = G[H + (a + d)\cos\theta] = T_m\left(\frac{\lambda}{d}\right)^3 + \frac{T_m \gamma_{sl}}{\rho_s q}\mathcal{K}, \tag{26}$$

written here in dimensional form and with H redefined to symbolize the distance of the center of the particle (soil grain) behind the 0 °C isotherm. The solid–melt interface has surface energy γ_{sl} and curvature $\mathcal{K}$, measured positive if the interface is convex toward the water. The final term in Eq. (26) represents the Gibbs–Thomson depression of the bulk freezing temperature at a curved interface. The analysis of Section 26.5 was developed under the assumption that this latter term is negligible, which is appropriate if the isolated, rejected particle is sufficiently large (Chernov et al., 1977). Within a porous medium (soil), this term plays an important role in determining the location of the ice–water interface.

It is necessary to consider the interaction within and between two regions: an interfacial region near the base of a soil grain and the free region between grains [Fig. 26.5(b)]. We proceed from here with the assumption that $a \ll H$, i.e., that the front of the ice lens lags behind the 0 °C isotherm by a distance that is much greater than the size of a soil grain. In the interfacial region, the film thickness d is small, the interface conforms closely to the soil grain, and Eq. (26) can

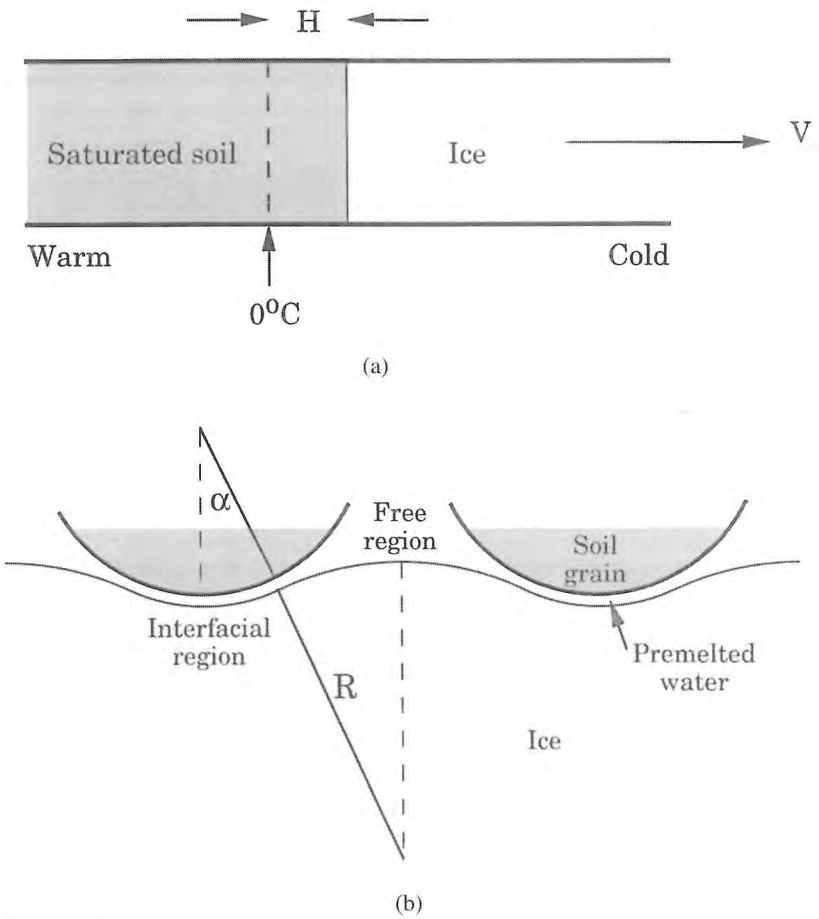

Figure 26.5. (a) Plan view of an experiment (T. Ishizaki, private communication) in which water-saturated soil, placed between two microscope slides, is pulled at constant speed V through a temperature gradient. If the pulling speed is sufficiently slow, then a steady state can be acheived in which a single ice lens rejects all the soil in advance of it. The ice-lens front lags behind the 0°C isotherm. (b) A magnified sketch of the ice-lens front showing soil grains being pushed ahead of the ice by the intermolecular forces in the interfacial region. The ice–water meniscus adopts a constant curvature in the free regions between soil grains.

be approximated to

$$\left(\frac{\lambda}{d}\right)^3 = \frac{GH}{T_m} + \frac{2\gamma_{sl}}{\rho_s q a}. \tag{27}$$

Equation (1) is modified at a curved interface but Eq. (3) still holds, whence

$$p_T = \frac{\rho_s q G}{T_m} H. \tag{28}$$

The integral of the pressure is not dominated by the neigborhood of $\theta = 0$, as it was for the isolated particle, and cannot therefore be approximated asymptotically in the same way. Rather, the upper limit of integration is set to $\theta = \alpha$, where the angle α is determined by matching with

the free region. The total thermomolecular force is then calculated to be

$$F_T = \int_0^{\alpha} (p_T \cos\theta) 2\pi a^2 \sin\theta \, d\theta = \frac{\pi a^2 \rho_s q G}{T_m} H(1 - \cos^2\alpha)$$
$$\sim \frac{\pi a^2 \rho_s q G}{T_m} H\alpha^2 \quad (\alpha \ll 1). \tag{29}$$

The lubrication pressure is obtained from Eqs. (15), with Eq. (27) for d, to be

$$p_l - p_f = -\frac{6\mu a^2 V G}{\lambda^3 T_m}(H + \Gamma)(\cos\theta - \cos\alpha),$$

where $\Gamma = 2\gamma_{sl} T_m / \rho_s q G a$, whence the net lubrication force is found to be

$$F_\mu = -\frac{\pi\mu a^4 V G}{\lambda^3 T_m}(H + \Gamma)(4 - 6\cos\alpha + 2\cos^3\alpha)$$
$$\sim -\frac{3\pi\mu a^4 V G}{2\lambda^3 T_m}(H + \Gamma)\alpha^4 \quad (\alpha \ll 1). \tag{30}$$

Within the free region, the van der Waals interaction is negligible and Eq. (26) is approximated by

$$H = \Gamma \frac{a}{R}, \tag{31}$$

where R is the constant radius of curvature of the ice–water interface. There is a complicated geometrical problem within the free region to determine the shape of the interface, which makes zero contact angle with the soil grains. However, simple considerations of geometry and scaling lead to the approximate relationship $\alpha \sim a/R$, whence

$$\alpha \sim \frac{H}{\Gamma}. \tag{32}$$

The thermomolecular and lubrication forces on a soil grain must balance the overburden force F_O applied to it, which for illustration here we take to be constant. Further, we consider only the case in which $\Gamma \gg H$. In dimensional terms, this inequality is $2\gamma_{sl} T_m / \rho_s \, qa \gg GH$, which indicates that the undercooling of the ice lens $\Delta = GH$ is much less than the Gibbs–Thomson undercooling arising from the curvature of a soil grain. Equivalently, the inequality means that the radius of curvature of the ice–water interface in the free region is much larger than the radius of a soil grain. In this case, the balance of forces leads to the equation

$$V = \frac{A}{9\pi\mu a^2}\left(\frac{2\gamma_{sl}}{a}\right)\left(\frac{T_m}{\rho_s q}\right)\frac{\Delta^3 - \Delta_c^3}{\Delta^4}, \tag{33}$$

where

$$\Delta_c = \left(\frac{F_O}{\pi a^2}\right)^{1/3}\left(\frac{2\gamma_{sl}}{a}\right)^{2/3}\frac{T_m}{\rho_s q}. \tag{34}$$

Figure 26.6 shows the possible steady growth rates V for a single ice lens as a function of the undercooling Δ. We see that a minimum undercooling Δ_c is required in order for the

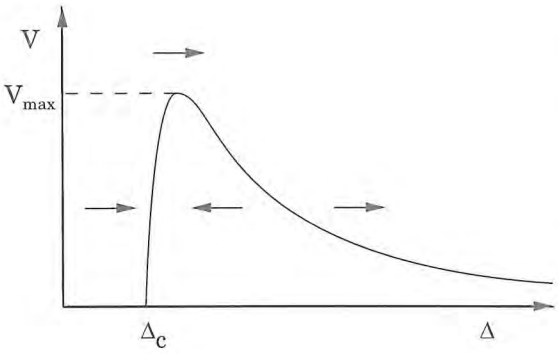

Figure 26.6. A graph of the possible steady states of single-ice-lens growth showing the undercooling of the ice-lens front $\Delta = GH$ corresponding to a given pulling speed V. The arrows show the directions in which the front migrates, which shows that the left-hand branch of solutions is stable, while the right-hand branch is unstable. If the pulling speed is too great then no steady state exists and the planar front recedes to positions of greater undercooling.

thermomolecular pressure to overcome the overburden. We also see that there are no steady solutions with a growth rate greater than

$$V_{\max} = \frac{A}{3.4^{4/3}\pi\mu a^2}\left(\frac{2\gamma_{sl}}{a}\right)^{1/3}\left(\frac{\pi a^2}{F_O}\right)^{1/3}. \tag{35}$$

A time-dependent analysis shows that the system evolves, as shown by the arrows in Fig. 26.6, which indicates that the left-hand branch of steady solutions is stable, the right-hand branch is unstable, and that the front of the ice lens recedes to colder temperatures if $V > V_{\max}$. It is anticipated that the planar ice-lens front will become unstable once its undercooling becomes too large, but proof of this awaits further study.

26.7. Epilog

The phenomenon of premelting gives rise to interesting fluid mechanical problems in which intermolecular interactions dictate both the pressure field driving a flow and the geometry of the flow domain. Confining our attention to van der Waals interactions, we have illustrated a few fundamental flows driven by premelting. The scale of premelted liquid films is of the order of nanometers but the pressures within them can be many tens of atmospheres. As a result, these microscopic flows can have enormous environmental consequences, shaping the landscape in cold regions of the Earth and having devastating effects on manmade structures built in such regions. The fluid-mechanical ideas presented here provide a basis for the development of macroscopic models of the deformation of partially frozen soils that can be used to predict these effects.

Acknowledgments

We are very grateful to Greg Dash and to Alan Rempel for their critical reading of the manuscript and to the Natural Environment Research Council of the UK and the National Science Foundation of the US for their support of our research.

References

Anderson, J. L. 1989. Colloid transport by interfacial forces. *Ann. Rev. Fluid Mech.* **21**, 61–99.

Azouni, M. A., Casses, P., and Sergiani, B. 1997. Capture or repulsion of treated nylon particles by an ice–water interface. *Colloids Surf. A* **122**, 199–205.

Azouni, M. A., Kalita, W., and Yemmou, M. 1990. On the particle behaviour in front of advancing liquid–ice interface. *J. Cryst. Growth* **99**, 201–205.

Chernov, A. A., Temkin, D. E., and Mel'nikova, A. M. 1977. The influence of the thermal conductivity of a macroparticle on its capture by a crystal growing from a melt. *Sov. Phys. Crystallogr.* **22**, 656–658.

Dash, J. G., Fu, H-Y., and Wettlaufer, J. S. 1995. The premelting of ice and its environmental consequences. *Rep. Prog. Phys.* **58**, 115–167.

Faraday, M. 1860. Note on regelation. *Proc. R. Soc. London* **10**, 440–450.

Gilpin, R. R. 1979. A model of the "liquid-like" layer between ice and a substrate with applications to wire regelation and particle migration. *J. Colloid Interface Sci.* **68**, 235–251.

Gilpin, R. R. 1980. Wire regelation at low temperatures. *J. Colloid Interface Sci.* **72**, 435–448.

Levich, V. G. 1962. *Physicochemical Hydrodynamics* (Prentice-Hall, Englewood Cliffs, NJ), p. 384.

Lipowsky, R. 1982. Critical surface phenomena at first-order bulk transitions. *Phys. Rev. Lett.* **49**, 1575–1578.

Lipowsky, R. 1984. Upper critical dimension for wetting in systems with long-range forces. *Phys. Rev. Lett.* **52**, 1429–1432.

Lipp, G. and Körber, Ch. 1993. On the engulfment of spherical particles by a moving ice–liquid interface. *J. Cryst. Growth* **130**, 475–489.

Lipp, G., Köber, Ch., and Rau, G. 1990. Critical growth rates of advancing ice–water interfaces for particle rejection. *J. Cryst. Growth* **99**, 206–210.

Löwen, H., Beier, T., and Wagner, H. 1989. Van der Waals theory of surface melting. *Europhys. Lett.* **9**, 791–796.

Mantovani, S., Valeri, S., Loria, A., and del-Pennino, U. 1980. Viscosity of the ice surface layer. *J. Chem. Phys.* **72**, 1077–1083.

Nye, J. F. 1967. Theory of regelation. *Philos. Mag.* **16**, 1249–1266.

Pötschke, J. and Rogge, V. 1989. On the behaviour of foreign particles at an advancing solid–liquid interface. *J. Cryst. Growth* **94**, 726–738.

Tabor, D. 1991. *Gases, Liquids and Solids*. (Cambridge U. Press, Cambridge).

Telford, J. W. and Turner, J. S. 1963. The motion of a wire through ice. *Philos. Mag.* **8**, 527–531.

Tyndall, J. 1858. On some physical properties of ice. *Proc. R. Soc. London* **9**, 76–80.

Wettlaufer, J. S. and Worster, M. G. 1995. Dynamics of premelted films: frost heave in a capillary. *Phys. Rev. E* **51**, 4679–4689.

Wettlaufer, J. S., Worster, M. G., Wilen, L. A., and Dash, J. G. 1996. A theory of premelting dynamics for all power law forces. *Phys. Rev. Lett.* **76**, 3602–3605.

Wilen, L. A. and Dash, J. G. 1995. Frost heave dynamics at a single crystal interface. *Phys. Rev. Lett.* **74**, 5076–5079.

Wilen, L. A., Wettlaufer, J. S., Elbaum, M., and Schick, M. 1995. Dispersion force effects in interfacial premelting of ice. *Phys. Rev. B* **52**, 426–433.

Yih, C-S. 1986. Movement of liquid inclusions in soluble solids: an inverse Stokes' law. *Phys. Fluids* **29**, 2785–2787.

Yih, C-S. 1987. Convective instability of a spherical fluid inclusion. *Phys. Fluids* **30**, 36–44.